ACS OMEGA

Open Access

http://pubs.acs.org/journal/acsodf

Article

A New Evaluation Method of Recoverable Reserves and Its Application in Carbonate Gas Reservoirs

Mengfei Zhou, Xizhe Li,* Yong Hu,* Chang He, Qimin Guo, Yize Huang, Xiangyang Pei, and Nijun Qi

Cite This: *ACS Omega* 2024, 9, 23649−23661

Read Online

ACCESS | Metrics & More | Article Recommendations

ABSTRACT: The propagation pattern of pressure drawdown effectively reflects the recoverable reserves range around the gas well and serves as a crucial basis for development strategies. However, it is not easy to detect the pressure propagation boundary near the producing well, especially in low-permeability reservoirs where the drainage radius is small. Physical simulation experiments can serve as a crucial method as the whole pressure profile and gas rate can be obtained in real time. Using long core plugs with permeabilities of 2.300 mD, 0.486 mD, and 0.046 mD, physical simulation experiments were carried out under varying initial water saturation (Swi) conditions of 0%, 20%, 40%, and 55% to observe the dynamic variations in pressure profiles of the core plugs during pressure depletion. Based on the material balance equation and pressure profile characteristics of the core plugs, a method for evaluating recoverable reserves within a well-spacing radius through laboratory experiments was proposed and performed. Mechanism analysis was conducted based on mercury injection tests, and suggestions for enhancing gas recovery were presented. Research findings indicate that lower permeability, higher initial water saturation, and higher abandonment gas rates result in reduced reserve utilization range and degree. Under abandoned gas rate conditions, for type I and II rocks, the pore radius is primarily distributed between 0.1 and 1 μm, the pressure drawdown can reach the well-spacing radius of 600 m, and the ultimate recovery efficiencies are more than 70.6%. For type III rocks, the pore radius mainly falls below 0.1 μm, the drainage radius is smaller than 10 m with Swi greater than 40%, and the ultimate recovery is below 10%. This paper provides an experimental method for recoverable reserves evaluation while formulating gas reservoir development strategies before well testing.

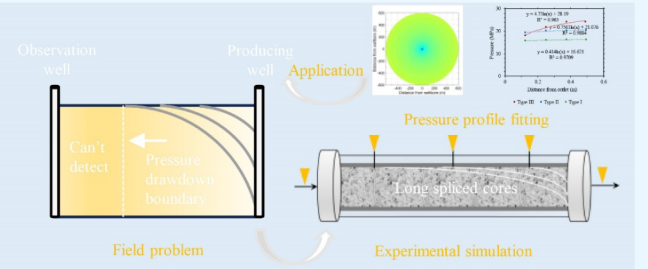

1. INTRODUCTION

Natural gas is a vital energy resource used extensively in heating, power generation, industrial production, transportation, and various other sectors.[1−3] As global demand for clean energy continues to rise, the extraction and utilization of natural gas have become increasingly important.[4,5] In this context, the assessment of gas reservoir recoverable reserves has become a critical issue in the natural gas industry. The evaluation of recoverable reserves in a gas reservoir aims to determine the economically producible natural gas reserves in a specific reservoir or gas field, providing essential information for development and production decision-making.[6−10]

Methods for assessing the original geological reserves and original recoverable reserves of gas reservoirs primarily include the material balance method, pressure-drop method, elastic two-phase method, decline curve analysis, and predictive modeling. Both the material balance method and pressure-drop method are based on the principle of mass conservation, estimating recoverable reserves by considering the relationships between gas production, water influx, and the changes in rock and fluid elastic expansion and pressure, using cumulative gas production and pressure data.[11−16] The elastic two-phase method evaluates the original geological reserves controlled by gas wells during the pseudosteady-state phase following the initiation of gas production, using the downhole flowing pressure and cumulative production.[17,18] The decline curve analysis is suitable for gas reservoirs entering the decline phase, rapidly estimating production and reserves by fitting historical production data.[19−22] While this method is relatively simple, it may not be suitable for new wells or complex reservoirs due to a lack of historical production data or the neglect of reservoir complexity.

Predictive modeling methods can be classified into two types. One is the single-peaked cycle models, which are established based on production vs time relationships. These models include the generalized Weng model,[23] Weibull model,[24,25] Rayleigh model,[26] Hubbert model,[27,28] and multipeak model.[29] The other is the cumulative growth models established based on

Received: February 9, 2024
Revised: April 25, 2024
Accepted: April 29, 2024
Published: May 17, 2024

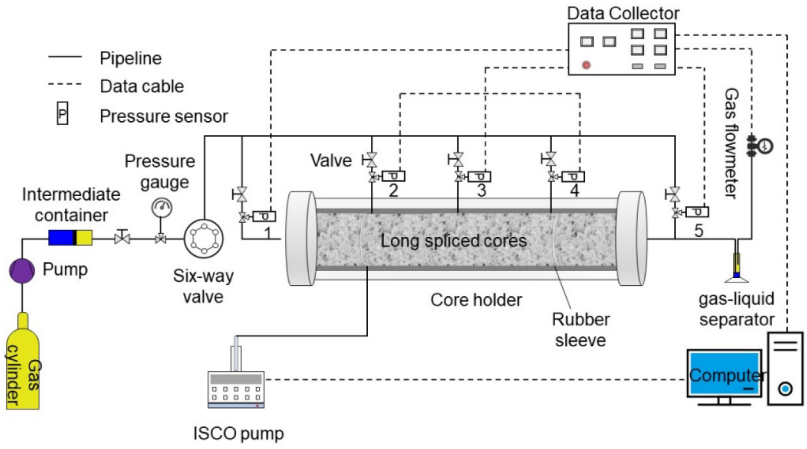

Figure 1. Schematic diagram of physical simulation experimental system.

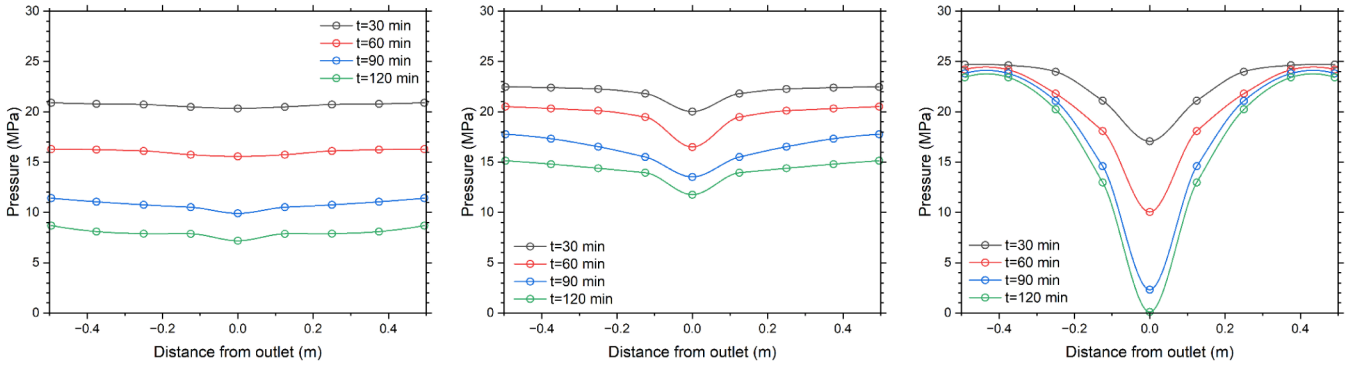

(a) Type I, K=2.300 mD (b) Type II, K=0.486 mD (c) Type III, K=0.046 mD

Figure 2. Pressure drawdown dynamics of three types of rock (Swi = 55%).

cumulative production vs time relationships.[30,31] These models are fitted using historical data to verify their applicability and accuracy and are used to predict production and remaining recoverable reserves.

The aforementioned methods for assessing recoverable reserves are typically applied when data on pressure and production are available from developed gas reservoirs, making them challenging to use for early stage evaluations. For reservoirs with low permeability, where gas flow capability is weak and pressure drawdown mainly occurs in the near-wellbore formation, reaching a pseudosteady state is difficult.[32−34] This also renders traditional assessment methods inapplicable.

It is possible to detect the pressure profile and spend less time and investment in the laboratory. To assess the recoverable reserves of reservoirs with different petrophysical properties, we conducted physical simulation experiments on three types of core samples with different permeabilities under varying water saturation conditions. By monitoring pressure changes at different locations within the core samples, we investigated the recoverable reserve characteristics of reservoirs with different properties. We established a recoverable reserve evaluation method based on the principles of material balance and physical simulation experiments. We then assessed the recoverable reserves under different abandonment conditions and proposed strategies to improve the degree of recoverable reserves for reservoirs with different properties.

2. MATERIALS AND METHODS

2.1. Experimental Method. A comprehensive physical simulation experimental system for studying long-core depletion was employed (Figure 1). By inserting the pressure sensor probes into the rubber sleeve of the core holder, real-time pressure data from the interior of the core was collected. Given that the lower limits of petrophysical parameters for effective carbonate gas reservoirs are 2.68%, 0.042mD,[35] three groups of long core plugs, each measuring 50 cm in length, were selected with permeability ranges of 1−10 mD (type I), 0.1−1 mD (type II), and 0.01−0.1 mD (type III), resulting in average permeabilities of 2.300 mD, 0.486 mD, and 0.046 mD, respectively. Under varying initial water saturations (Swi) of 0%, 20%, 40%, and 55%, depletion tests with constant gas production rates were conducted to simulate physical scenarios. See details about the experimental procedures in reference 36. These experiments provided insights into the pressure profile changes along the long core plugs.

As shown in Figure 2, taking Swi = 55% as an example, the pressure profile variations during the depletion processes of the three types of long cores are displayed. To show the complete pressure drop funnel, the pressure profile on the negative semiaxis was made by the symmetry method. This unveils the pressure drawdown propagation characteristics within reservoirs of different permeabilities. The results indicate significant differences in pressure profile features during the depletion of reservoirs with distinct permeabilities, suggesting notable variations in their reserve utilization behaviors. For the type I

https://doi.org/10.1021/acsomega.4c01323
ACS Omega 2024, 9, 23649−23661

reservoir with a permeability of 2.300 mD, the reservoir pressure uniformly declines, the pressure drawdown propagates over a considerable distance, and the pressure profile remains remarkably smooth (Figure 2a). Conversely, for the type II reservoir with a permeability of 0.486 mD, though the pressure drawdown propagation distance remains considerable, the pressure drawdown near the wellbore is more pronounced, leading to an altered pressure profile shape (Figure 2b). Notably differing from the type I and type II reservoirs, the pressure profile characteristics of the type III reservoir with a permeability of 0.046 mD are distinct (Figure 2c). The pressure profile is steep, even when the bottom-hole pressure (outlet pressure in the experiment) drops to 0.1 MPa, the distal reservoir pressure barely decreases, indicating a limited propagation distance for the pressure drawdown and a small range for reserve utilization. Therefore, it can be inferred that the extent of reserve utilization is influenced not only by physical boundaries but also by reservoir petrophysical properties.

As illustrated in Figure 3, taking the pressure profiles of the three types of long cores at t = 60 min as an example, a

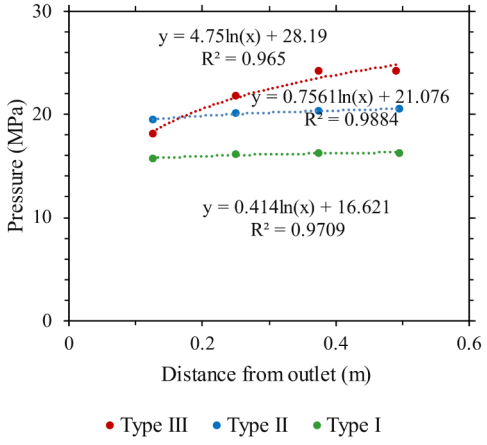

Figure 3. Fitting results of pressure profiles of three types of rock at t = 60 min.

logarithmic function fitting relationship is observed between reservoir pressure and distance from the outlet end. This fitting method, identified through the scatter fitting of pressure profiles, will be extensively employed in subsequent sections for predicting the distribution of reservoir pressure in actual gas reservoirs. This method will also be used to evaluate the range and degree of reserve utilization.

2.2. Evaluation Theory. In the absence of a natural aquifer drive in a closed gas reservoir, it can be treated as a volumetric reservoir. According to the principle of material balance, in a volumetric gas reservoir, the pressure decrease resulting from production triggers the expansion of gas, rock, and connate water within the reservoir. The cumulative effects of these components are equivalent to the in-place cumulative gas production of the reservoir. Comparatively, the expansion of rock and connate water can be negligibly small in comparison to gas expansion. Therefore, the pressure decline in the gas reservoir is solely related to the cumulative gas production, allowing for the calculation of gas recovery using pressure changes.[11]

Assuming that a producer is located at the center of a homogeneous and uniform-thickness reservoir, the reservoir pressure starts to decline after gas production. At a certain moment, the pressure profile is depicted in Figure 4. The enclosed area beneath the pressure profile (highlighted in

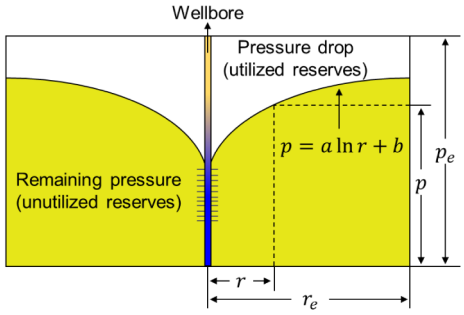

Figure 4. Schematic of recovery evaluation method of volumetric gas reservoirs.

yellow) represents the remaining reserves, while the portion above the pressure profile (in white) represents the utilized reserves. The total area encompasses the original reserves.

In Figure 4, where p_e denotes the initial reservoir pressure, r_e represents the well-spacing radius, and p signifies the reservoir pressure at a distance r from the wellbore. To facilitate calculations and applications, nondimensionalization will be applied to p and r:

$$p_D = p/p_e \tag{1}$$

$$r_D = r/r_e \tag{2}$$

Based on the aforementioned method for evaluating gas recovery, the gas recovery R within r_e is calculated as the area of the yellow region divided by the total area. This is expressed by the following equation:

$$R = 1 - \int_0^1 p_D \, dr_D \tag{3}$$

As depicted in Figure 3, by fitting the pressure profiles obtained from the physical simulation experiments, a robust logarithmic function relationship is identified between reservoir pressure p_D and distance from the wellbore r_D, as represented by the equation:

$$p_D = a \ln r_D + b \tag{4}$$

Substituting eq 4 into Eq 3, we obtain the formula for evaluating gas recovery within r_e:

$$R = 1 - \int_0^1 (a \ln r_D + b) dr_D \tag{5}$$

2.3. Evaluation Steps. (1) Utilize the aforementioned physical simulation experiment method to simulate reserve utilization using long cores and acquire real-time pressure variations along the core length.

(2) Select pressure profiles from different production stages for function fitting, enabling the assessment of reserve utilization during various production phases. This study involves evaluating gas recovery under three scenarios: the bottom-hole pressure droping to 5 MPa is selected as the abandoned pressure condition, the gas production rate droping to the initial rate of 15% as the abandoned gas rate condition, and no gas production as the extreme condition to carry out the gas recovery evaluation.

(3) To eliminate end effects and facilitate function fitting, choose four pressure points excluding the outlet end for function

https://doi.org/10.1021/acsomega.4c01323
ACS Omega 2024, 9, 23649−23661

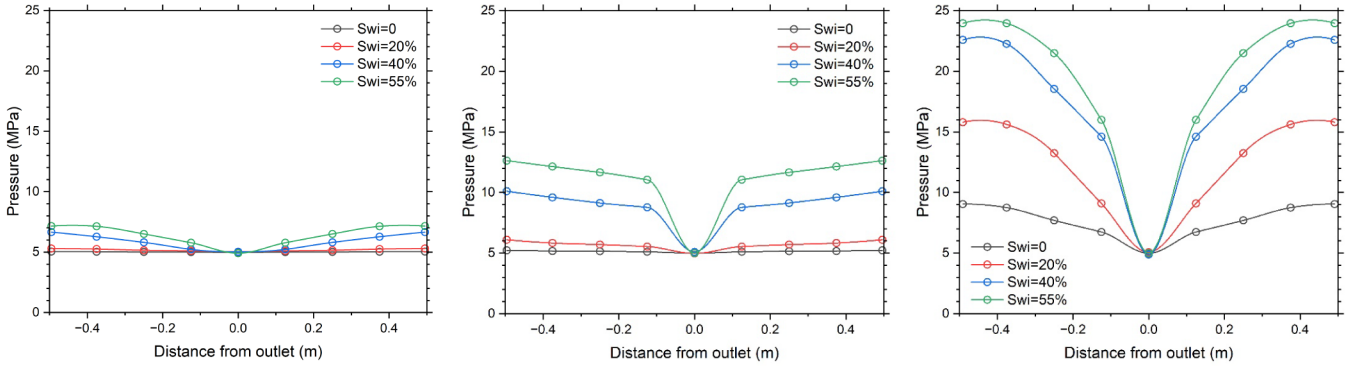

(a) Type I, K=2.300 mD (b) Type II, K=0.486 mD (c) Type III, K=0.046 mD

Figure 5. Pressure profiles under abandoned pressure condition.

fitting. Obtain the functional relationship between reservoir pressure and distance from the wellbore, as illustrated in Figure 3. From this, deduce the values of parameters'*a*' and'*b*' in eq 4.

(4) With the obtained values of'*a*' and'*b*,' combine them with the actual original reservoir pressure to determine the reserve utilization range and pressure distribution around the production well. Implement two-dimensional visualization of the pressure distribution.

(5) Once the reserve utilization range and pressure distribution around the production well are established, assess gas recovery within the well-spacing radius in such reservoirs using eq 5.

3. EVALUATION RESULTS

3.1. Abandoned Pressure Condition. When the bottom-hole pressure is very low, the wellhead pressure also becomes low. However, when the wellhead pressure falls below the pipeline transportation pressure, natural gas will be unable to enter the gathering plant. In such cases, it becomes necessary to employ booster compressors at the wellhead to maintain the required gas transportation pressure. Here, we are assuming that under the condition of a bottom-hole pressure of 5 MPa, without wellhead boosting, gas wells will not be able to supply gas to the gathering station because of their inability to meet the required transportation pressure.

3.1.1. Pressure Profiles and Functional Fitting Results. Based on the results of the physical simulation experiments, when the pressure at the outlet end of the long core drops to 5 MPa, the pressure profiles for the three types of rocks at various initial water saturations are illustrated in Figure 5. Using logarithmic fitting on the pressure profiles shown in Figure 5, a functional relationship between pressure and the distance from the outlet is obtained. Consequently, values for'*a*' and'*b*' are deduced. The outcomes are presented in Table 1.

3.1.2. Remaining Pressure Distributions. Taking the Lei 1 gas reservoir in the Sichuan Basin as an example, with an original reservoir pressure of 40 MPa and a well-spacing radius of 600 m, we can use the logarithmic functional relationship obtained from the physical simulation experiments under the abandoned pressure condition to calculate the pressure distribution and pressure drawdown propagation distance in the actual gas reservoir. This calculation will allow us to create a top-view visualization, as demonstrated in Figure 6.

From Figure 6, it can be observed that when the reservoir does not contain connate water, the remaining reservoir pressure for type I and type II is low, and there's no noticeable pressure gradient. Although the type III reservoir exhibits a pressure drawdown within the well control range, the remaining pressure is high. For the type III reservoir, the remaining boundary pressure of the well-spacing radius reaches 21.48 MPa, with a significant pressure drawdown concentrated within 100 m around the producer. When Swi = 20%, the type II reservoir shows a distinct pressure gradient, and the pressure drawdown for the type III reservoir is confined within a radius of about 48 m around the producer, indicating a very limited depletion range. At Swi = 40%, only a small area within 8 m around the production well shows a pressure drawdown for the type III reservoir, implying that the reservoir is difficult to exploit and lacks development value using conventional techniques. On the other hand, the remaining pressures for type I and type II reservoirs notably increase, with increased pressure gradients. The remaining boundary pressures of the well-spacing radius are 13.87 and 17.73 MPa, respectively. When Swi rises to 55%, the remaining pressures in the reservoir are high, and the boundary pressures for type I and type II reservoirs decrease to 14.89 and 20.44 MPa, respectively.

Table 1. Function Fitting Results of Pressure Profiles Under Abandoned Pressure Condition

type of reservoir	Swi (%)	*a*	*b*	R^2
I	0	0.0295	5.0579	0.9299
	20	0.1418	5.3801	0.9343
	40	1.0259	7.3059	0.9874
	55	1.0735	8.0197	0.9678
II	0	0.0762	5.2631	0.9598
	20	0.3727	6.2719	0.8877
	40	0.9280	10.594	0.9257
	55	1.1152	13.305	0.9778
III	0	1.7469	10.310	0.9808
	20	5.1565	20.086	0.9697
	40	6.1973	27.488	0.9737
	55	6.1379	29.262	0.9476

3.1.3. Recovery Efficiency. Based on the relationship between reservoir pressure and distance from the wellbore shown in Figure 6, the recovery of reservoirs with different permeabilities under varying initial water saturations is evaluated within a well-spacing radius of 600 m, as depicted in Figure 7.

The results indicate that type I and type II reservoirs exhibit higher gas recovery. As initial water saturation increases, the gas recovery decreases. However, even at a high initial water saturation of 55%, the gas recovery remains above 51.7%. In contrast, type III reservoirs demonstrate a very low gas recovery,

https://doi.org/10.1021/acsomega.4c01323
ACS Omega 2024, 9, 23649−23661

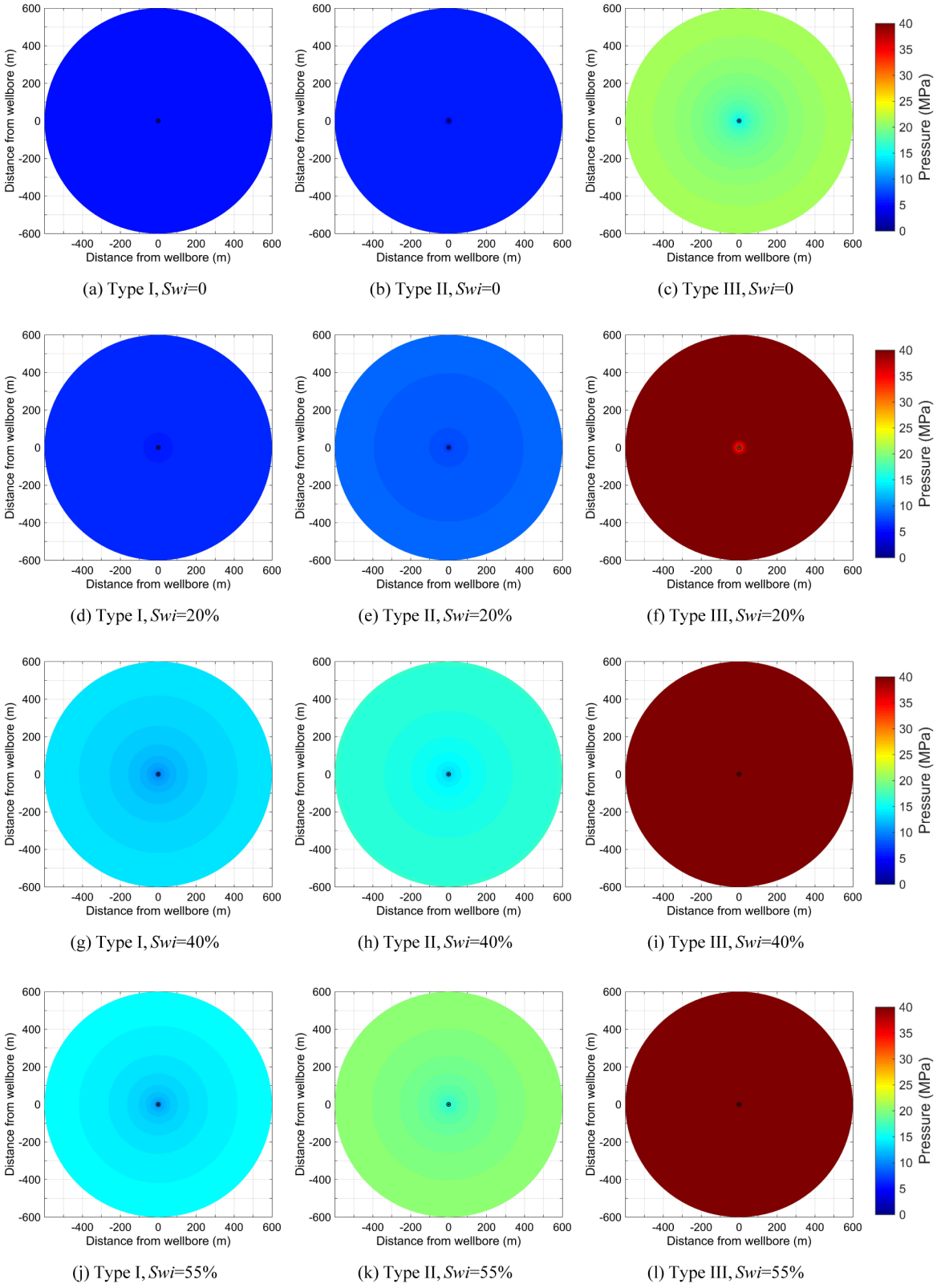

Figure 6. Top view of pressure distribution under abandoned pressure.

particularly under conditions of high initial water saturation. Even at a water saturation of only 20%, the gas recovery is merely 1.0%. This suggests that reservoirs of this type pose significant challenges for effective reserve utilization.

3.2. Abandoned Gas Rate Condition. When the daily production rate of a gas well is very low, the economic benefits of continued production decrease significantly. In this study, an abandoned gas rate condition is considered when the gas

https://doi.org/10.1021/acsomega.4c01323
ACS Omega 2024, 9, 23649−23661

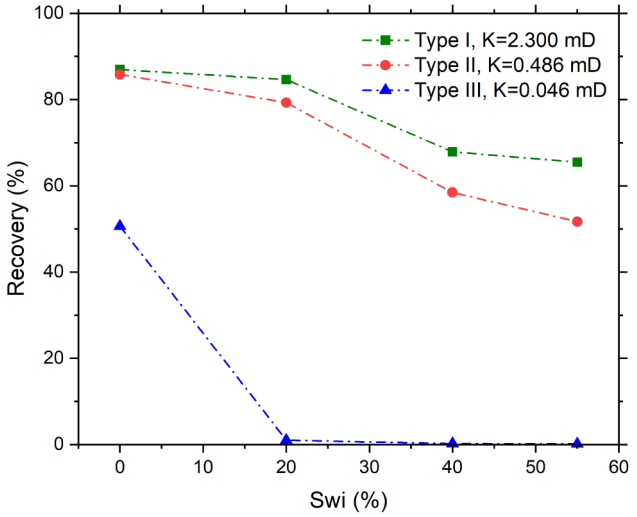

Figure 7. Recovery at a well-spacing radius of 600 m under abandoned pressure.

production rate drops to 15% of the gas production rate during the stable production period.

3.2.1. Pressure Profiles and Functional Fitting Results. Based on the results of the physical simulation experiments, pressure profiles under the abandoned gas rate condition, as depicted in Figure 8, were plotted. Through logarithmic function fitting, functional relationships between pressure and distance from the outlet under this condition were obtained. These relationships are presented in Table 2.

3.2.2. Remaining Pressure Distributions. Based on the functional relationships between reservoir pressure and distance from the wellbore under abandoned gas rate conditions (Table 2), the pressure distribution characteristics within a well-spacing radius of 600 m are determined as shown in Figure 9.

From Figure 9, it is evident that the remaining pressure distribution characteristics for type I and type II reservoirs are quite similar. They both exhibit very low remaining reservoir pressures and small pressure gradients. Even when Swi = 55%, the pressure drawdown can propagate to the boundaries of the well-spacing radius. However, for type II reservoirs, the remaining pressure is slightly higher compared to type I reservoirs.

In contrast, the remaining pressure distribution characteristics for type III reservoirs are notably different from the first two types. Even if there is no connate water in the reservoir, the boundary pressure of the type III reservoir still retains a remaining pressure of 12.80 MPa. When Swi = 20%, there is no pressure drawdown beyond a distance of 371 m from the producer, indicating a reserve utilization radius of 371 m. However, for Swi ≥ 40%, the drainage radius becomes less than 10 m, implying that under conventional technical conditions, the reservoir does not hold significant development value.

Table 2. Function Fitting Results of Pressure Profiles Under Abandoned Gas rateCondition

type of reservoir	Swi (%)	*a*	*b*	R^2
I	0	0.0829	0.2642	0.9357
	20	0.2561	0.6497	0.9451
	40	0.5855	1.5788	0.9771
	55	1.1540	3.2507	0.9495
II	0	0.1816	0.6812	0.9208
	20	0.5908	1.8956	0.9444
	40	0.8027	4.3005	0.9354
	55	1.1718	5.4180	0.9954
III	0	1.3183	4.3649	0.9853
	20	4.6146	12.705	0.9719
	40	8.1585	26.162	0.9732
	55	7.9079	30.116	0.9439

3.2.3. Recovery Efficiency. Based on the pressure distribution characteristics in Figure 9, the recovery of reservoirs with different permeabilities under varying initial water saturations within a well-spacing radius of 600 m is evaluated and depicted in Figure 10.

The results demonstrate that under abandoned gas rate condition, type I and type II reservoirs exhibit very high gas recovery. They are relatively less influenced by initial water saturation. Even at Swi = 55%, the gas recovery remains above 70.6%. In contrast, the gas recovery for type III reservoirs remains low under the same condition. They are significantly affected by connate water. When there is no connate water in the reservoir, the gas recovery for type III reservoirs can reach 71.3%. However, with a Swi = 20%, the gas recovery drops substantially to 7.1%. As initial water saturation continues to increase, the gas recovery drops below 1%.

3.3. Extreme Condition. The extreme condition refers to a scenario in which the gas production rate at the outlet of the physical simulation experiment is reduced to zero, rendering the core incapable of producing gas. Under this circumstance, the

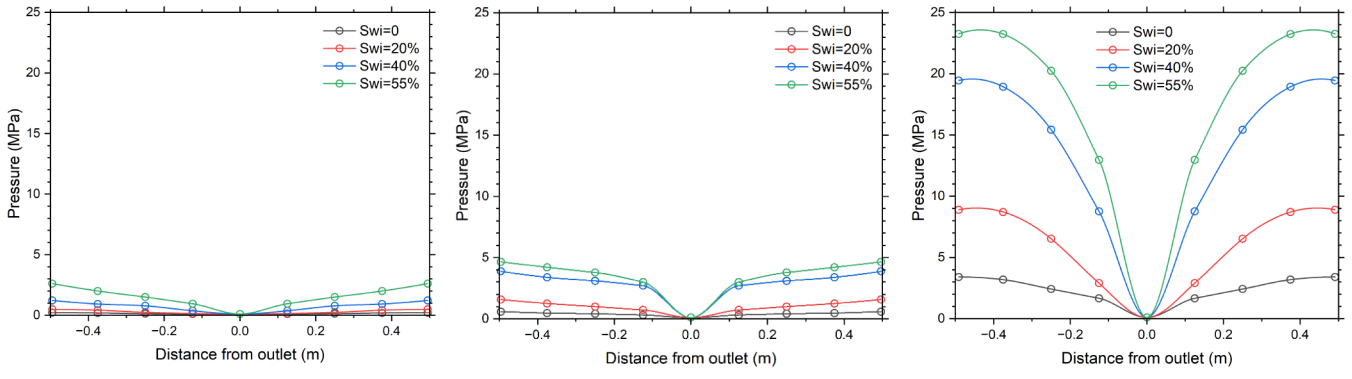

(a) Type I, K=2.300 mD (b) Type II, K=0.486 mD (c) Type III, K=0.046 mD

Figure 8. Pressure profiles under abandoned gas rate condition.

https://doi.org/10.1021/acsomega.4c01323
ACS Omega 2024, 9, 23649−23661

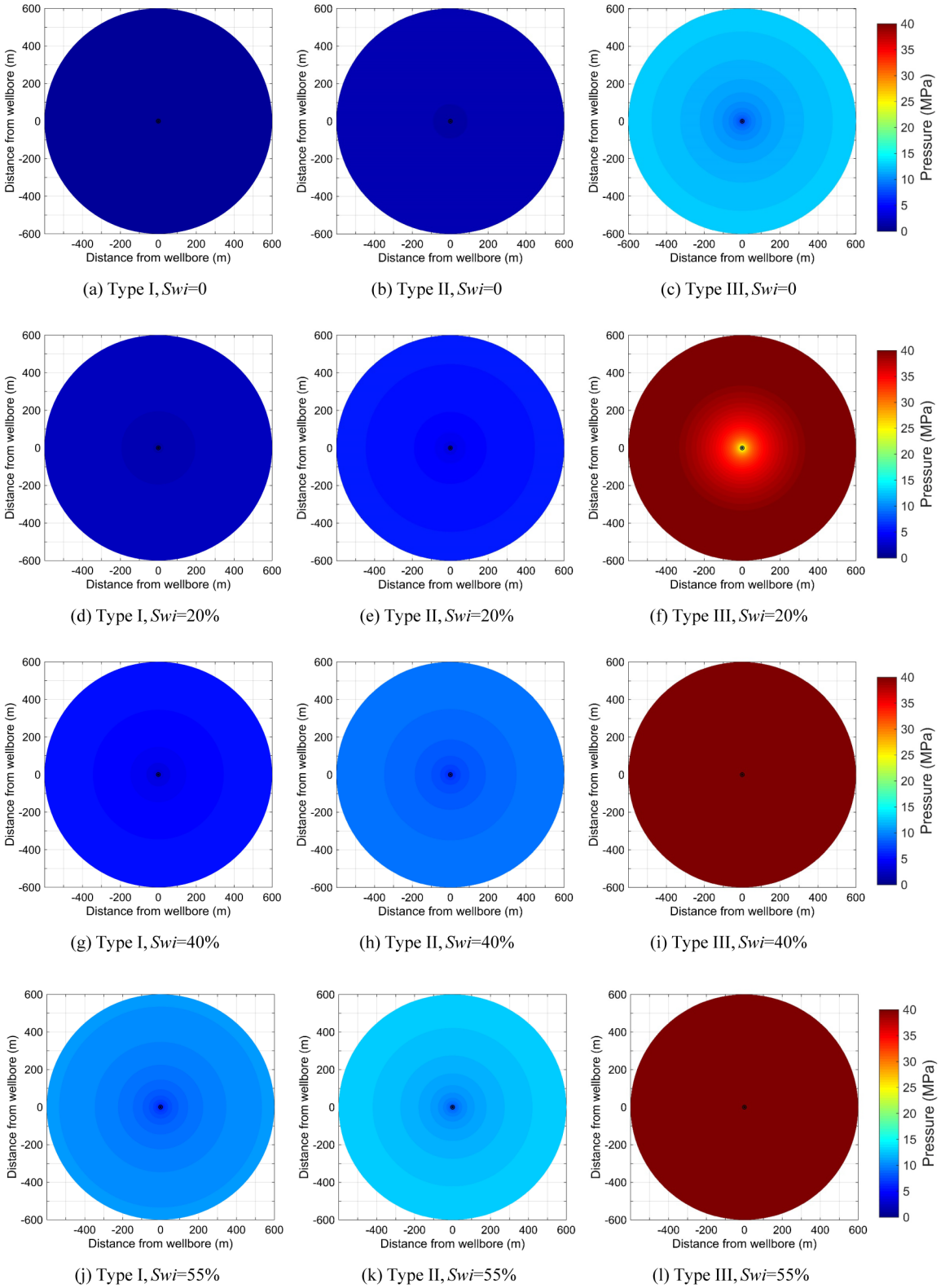

Figure 9. Top view of pressure distribution under abandoned gas production rate.

obtained gas recovery should theoretically represent the maximum achievable gas recovery.

3.3.1. Pressure Profiles and Functional Fitting Results. Based on the results of the physical simulation experiments, pressure profiles under extreme conditions, as illustrated in Figure 11, were plotted. Through logarithmic function fitting, functional relationships between reservoir pressure and distance under this condition were obtained. These relationships are presented in Table 3.

3.3.2. Remaining Pressure Distributions. Based on the functional relationships between reservoir pressure and distance from the wellbore under the extreme condition (Table 3), the

https://doi.org/10.1021/acsomega.4c01323
ACS Omega 2024, 9, 23649−23661

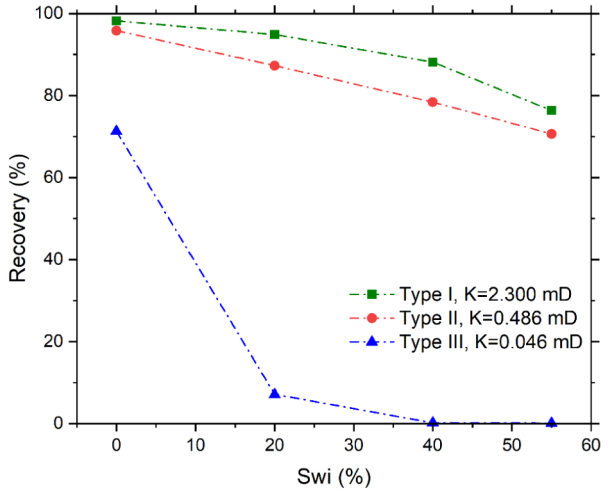

Figure 10. Recovery at a well-spacing radius of 600 m under abandoned gas production rate.

pressure distribution characteristics within a well-spacing radius of 600 m were determined, as shown in Figure 12.

From Figure 12, it can be observed that when there is no connate water in the reservoir, the remaining pressures for all three types of reservoirs are less than 1 MPa, indicating thorough and balanced depletion. For type I reservoirs, with initial water saturations of 20%, 40%, and 55%, the boundary pressures decrease to 0.45, 1.79, and 4.59 MPa, respectively. The remaining pressures are relatively low, and the pressure gradients are small, suggesting a fairly balanced reserve utilization. Similarly, for type II reservoirs, with initial water saturations of 20%, 40%, and 55%, the boundary pressures decrease to 4.79, 5.33, and 5.34 MPa, respectively. The remaining pressures are low, and the pressure gradients are small, indicating a relatively balanced reserve utilization.

However, for type III reservoirs, with initial water saturations of 20%, 40%, and 55%, the boundary pressures of the well-spacing radius decrease to 22.30, 31.20, and 34.24 MPa, respectively. The remaining pressures are significantly higher, with a notable pressure gradient in the near-well region and a smaller gradient in the far-well region. This suggests an uneven reserve utilization with a small drainage volume.

3.3.3. Recovery Efficiency. Based on the pressure distribution characteristics in Figure 12, the recovery of reservoirs with different permeabilities under varying initial water saturations within a well-spacing radius of 600 m is evaluated and depicted in Figure 13.

Table 3. Function Fitting Results of Pressure Profiles Under Extreme Condition

type of reservoir	Swi (%)	*a*	*b*	R^2
I	0	0.0157	0.1327	0.9603
	20	0.0423	0.1844	0.9585
	40	0.1983	0.5228	0.9273
	55	0.4852	1.4897	0.9979
II	0	0.0862	0.2834	0.9199
	20	0.5320	1.3822	0.9875
	40	0.5247	1.9752	0.9862
	55	0.4631	2.3735	0.9763
III	0	0.1051	0.3131	0.9735
	20	2.4432	6.6678	0.9675
	40	3.1600	10.987	0.9896
	55	3.4300	12.303	0.9823

The results indicate that under extreme condition, type I and type II reservoirs exhibit very high gas recovery. The impact of initial water saturation on the gas recovery is minimal. Even at Swi = 55%, the gas recovery for type II and type I reservoirs can reach 87.8% and 89.7%, respectively. Under the extreme condition, the gas recovery for type III reservoirs is significantly affected by initial water saturation. With initial water saturations of 20%, 40%, and 55%, the gas recovery is 50.4%, 29.9%, and 23.0%, respectively.

3.4. Comparison and Analysis. As shown in Figure 14, within the well-spacing radius of 600 m, a comparative analysis of the gas recovery under the three abandonment conditions is conducted. Under the abandoned pressure condition, reservoirs have high remaining pressures and relatively lower gas recovery. Especially when Swi ≥ 40%. the gas recovery does not exceed 67.9%, indicating that the gas recovery has great room for improvement. For instance, when Swi = 40%, the increase in gas recovery due to transitioning from the abandoned pressure condition to the extreme condition is 28.1% for type I reservoirs, 29.5% for type II, and 29.7% for type III. Similarly, when Swi = 55%, the increase in gas recovery due to the same transition is 24.3% for type I, 36.1% for type II, and 22.8% for type III reservoirs. This analysis highlights that for water-bearing reservoirs, implementing measures such as wellhead pressure boosting can significantly enhance gas recovery by reducing reservoir abandonment pressures.

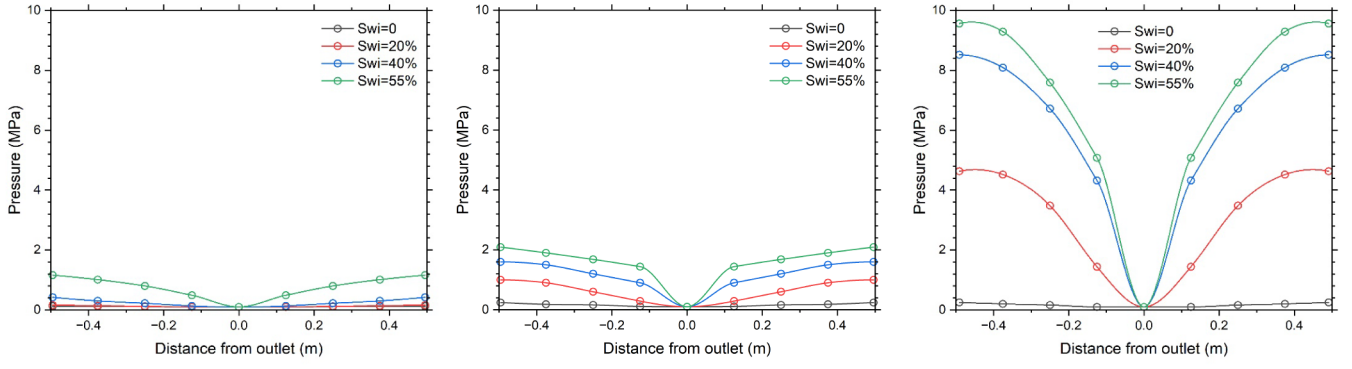

(a) Type I, K=2.300 mD (b) Type II, K=0.486 mD (c) Type III, K=0.046 mD

Figure 11. Pressure profiles under extreme condition.

https://doi.org/10.1021/acsomega.4c01323
ACS Omega 2024, 9, 23649−23661

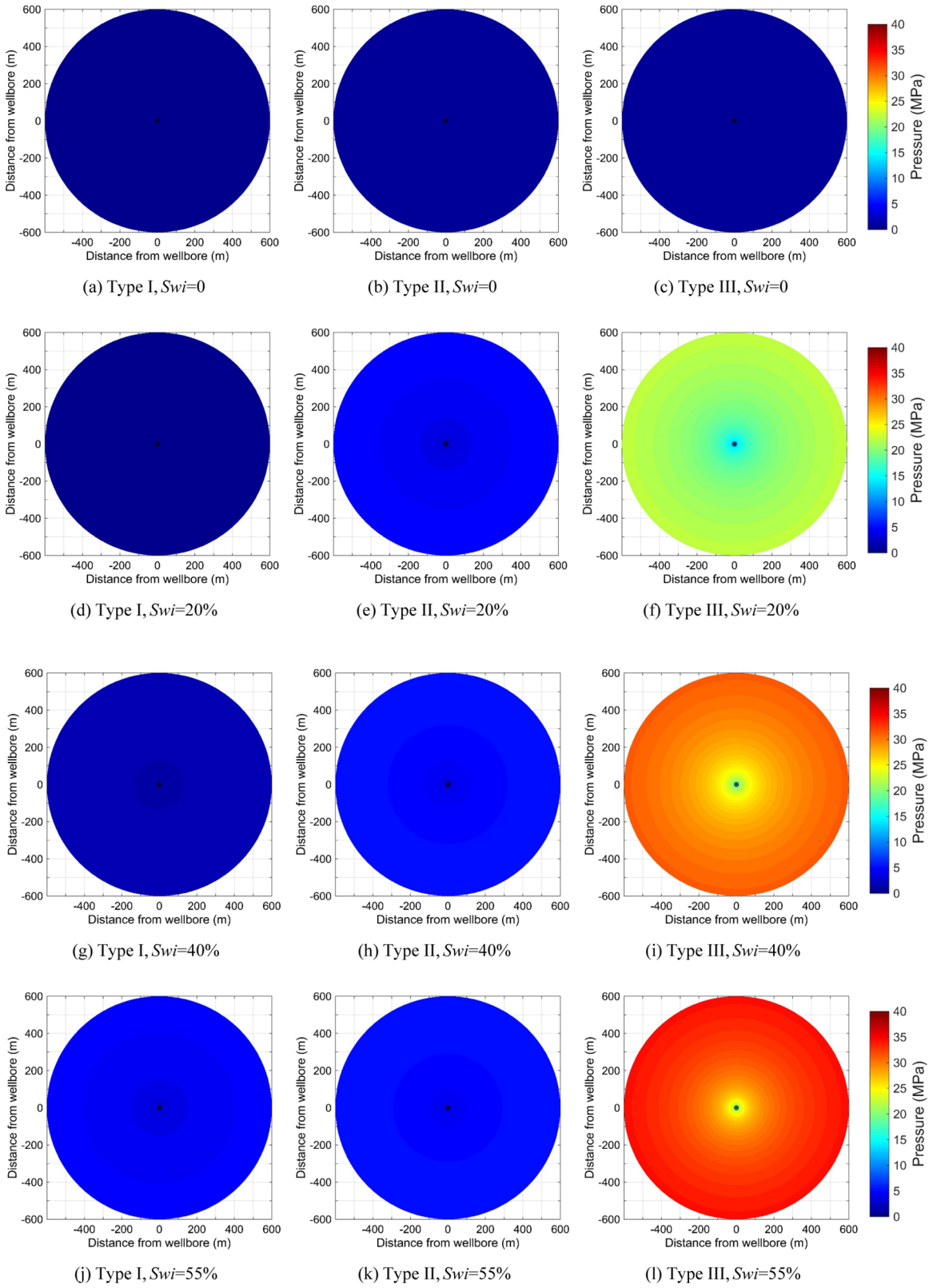

Figure 12. Top view of pressure distribution under extreme condition.

For type I and type II reservoirs, when Swi ≤ 20%, the gas recovery under the abandoned gas rate condition already exceeds 87.3%, leaving little room for significant improvement. Even if the abandonment condition is reduced to the extreme condition, the increase in gas recovery is limited to no more than 4.0%.

However, for type III reservoirs, which have low gas recovery when there is connate water, a significant improvement in gas recovery can be achieved by reducing the abandonment

https://doi.org/10.1021/acsomega.4c01323
ACS Omega 2024, 9, 23649−23661

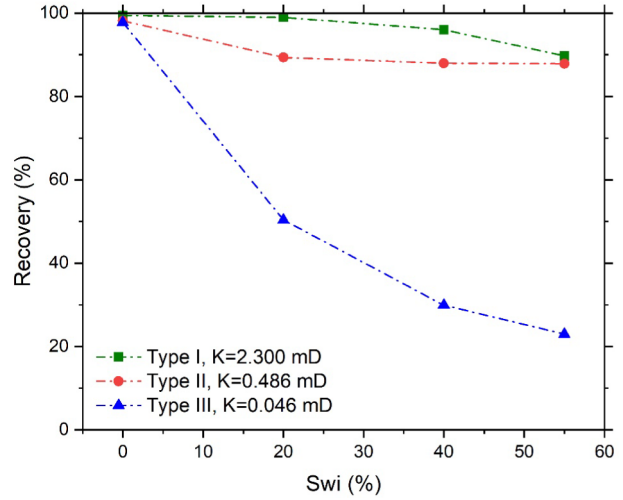

Figure 13. Recovery at a well-spacing radius of 600 m under extreme condition.

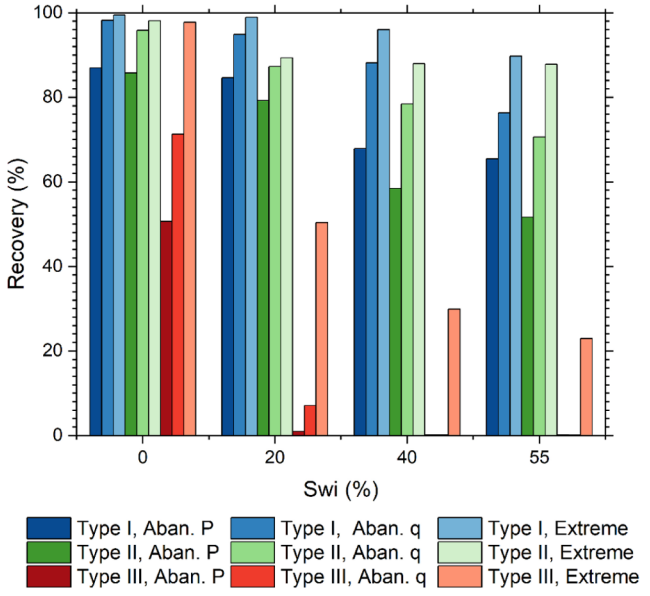

Figure 14. Comparison of recovery under different abandoned conditions.

condition. For instance, when the initial water saturations are 20%, 40%, and 55%, transitioning from the abandoned gas rate condition to the extreme condition increases the gas recovery by 43.2%, 29.7%, and 22.8%, respectively.

This analysis indicates that although water-bearing type III reservoirs have limited gas supply capacity, they contribute significantly to improving gas recovery during the low gas production stage.

In the actual development process of gas reservoirs, the type I reservoir with a permeability of 2.300 mD often has relatively low initial water saturation. Therefore, the reservoir can be fully exploited, leaving limited room for significant improvement in gas recovery. On the other hand, the type II reservoir with a permeability of 0.486 mD has a stronger gas-phase permeability within the matrix. However, the initial water saturation in this reservoir can vary widely, leading to notable differences in reserve utilization. When the Swi $\geq$ 40%, there is substantial potential for improving gas recovery. Thus, implementing techniques and measures to enhance gas recovery for this type of reservoir can yield significant results. It should be considered a primary target for increasing gas recovery.

In contrast, the type III reservoir with a permeability of 0.046 mD has small pores and throats, resulting in poor gas-phase flow capability when water-bearing. Additionally, these reservoirs typically have higher initial water saturation. Conventional measures struggle to improve their depletion extent.

4. RESULTS AND DISCUSSION

4.1. Characteristics and Mechanism. From the comparison in Figure 14, it is evident that the gas recovery of carbonate reservoirs is closely correlated with factors such as reservoir permeability, initial water saturation, and abandonment conditions. In general, the trend indicates that as permeability decreases, initial water saturation increases, and abandonment pressures rise, the corresponding gas recovery tends to decrease.

Pores and throats, serving as conduits for fluid permeation, directly influence the flow capacities of both gas and water phases. This, in turn, impacts the gas well productivity and the propagation of pressure drawdowns. Mercury injection testing stands as a classical method to characterize pore size distribution. This method was employed to perform tests on rocks of three permeability categories. By correlating the relationship between mercury injection pressure and pore radius, the pore radius distribution frequency curve illustrated in Figure 15 was obtained.

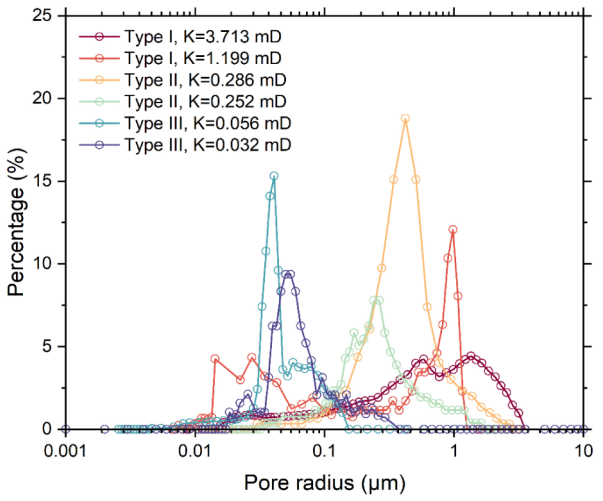

Figure 15. Pore size distributions of rocks with different permeabilities.

As permeability decreases, the curve gradually shifts toward the left, indicating a reduction in pore radius. Rocks of type I and type II exhibit larger pore radii, with more than 70% pores distributed within the range of 0.1 to 1 μm. Consequently, even with connate water present within the pores, gas can still flow freely. This attribute allows for pressure drawdown propagation over greater distances, resulting in a more balanced reserve utilization process. In contrast, rocks of type III possess significantly smaller pore radii, with at least 80% pores distributed below 0.1 μm. From the Young−Laplace equation, molecular dynamics simulation,[37,38] and visualization studies in pore scale,[39−41] in the presence of connate water within the pores, capillary pressures in type III rocks are about tens of times than those in type I and II rocks. Near the wellbore, the pressure difference between near-wellbore and bottom-hole pressures

https://doi.org/10.1021/acsomega.4c01323
ACS Omega 2024, 9, 23649−23661

enables gas to overcome capillary pressures and flow. However, as the distance from the wellbore increases, the pressure gradient diminishes. When the pressure difference falls below the capillary pressure, gas ceases to flow, causing an inability to propagate pressure drawdowns. Consequently, the distance over which pressure drawdowns propagate is minimal, indicating a confined range of reserve utilization.

4.2. Strategies and Suggestions. By combining physical simulation experiments with mathematical methods, the assessment of gas recovery for reservoirs with different permeabilities under various initial water saturations has been conducted. Based on the analysis of pressure drawdown characteristics and mechanisms within carbonate gas reservoirs, strategies and suggestions for improving gas recovery have been proposed:

(1) Reservoir permeability has a significant impact on gas recovery, especially for reservoirs with permeabilities less than 0.1 mD. Type III reservoirs with low permeability exhibit very low recovery within a well-spacing radius of 600 m. Such reservoirs can be improved through measures such as acidizing, hydraulic fracturing, deploying horizontal wells, and thickening well patterns to enhance gas flow capacity, expand effective well-controlled reserves, and increase the extent of reserve utilization within the well-spacing radius.

(2) Reservoir water saturation also exerts a substantial influence on gas recovery, particularly for type III reservoirs with permeabilities less than 0.1 mD. Within a well-spacing radius of 600 m, gas recovery sharply decreases with increasing initial water saturation. Therefore, during gas reservoir production, careful evaluation of the magnitude and distribution of connate water saturation is necessary. When perforating, layers with high initial water saturation should be avoided.

(3) Lowering the abandonment conditions of gas reservoirs can effectively enhance gas recovery, especially for reservoirs with higher initial water saturation and lower permeability. This approach yields significant improvements in gas recovery. Hence, using wellhead pressure boosting to reduce abandonment pressures in gas wells is recommended. This strategy prolongs the lifespan of gas wells, capitalizes on the contribution of the low-rate production phase to gas recovery, and enhances the extent of reserve utilization within the well-controlled area.

It is worth mentioning that different gas production rates will change the producing pressure differential and thus affect pressure propagation characteristics, even though it will not affect the difference between these three types of reservoirs, the effect of gas rates on the pressure profiles in a specific reservoir can be further investigated.

5. CONCLUSIONS

(1) Physical simulation experiments were conducted on carbonate rock with different permeabilities under various initial water saturations. This revealed the pressure drawdown characteristics and reserve utilization patterns of porous carbonate gas reservoirs. An integrated approach combining experimentation and mathematical analysis was developed, facilitating the visualization of reservoir pressure distribution and the assessment of well-spacing reserve utilization.

(2) The gas recovery of carbonate gas reservoirs is closely related to factors such as reservoir permeability, water saturation, and abandonment conditions. In general, lower permeability, higher initial water saturation, and higher abandonment pressure result in lower gas recovery.

(3) Type I and type II reservoirs exhibit balanced reserve utilization, long-pressure propagation distances, and high recovery. Additionally, further enhancing gas recovery can be achieved by reducing abandonment conditions. Type III reservoirs, however, present challenges in reserve utilization because of limited pressure propagation distance. To increase gas recovery in these cases, measures such as reservoir reformation to improve matrix flow capacity and deploying horizontal wells and infill drilling must be taken to expand reserve utilization and improve gas recovery.

AUTHOR INFORMATION

Corresponding Authors

Xizhe Li − *School of Engineering Sciences, University of Chinese Academy of Sciences, Beijing 100049, China; Institute of Porous Flow and Fluid Mechanics, Chinese Academy of Sciences, Langfang 065007, China; Research Institute of Petroleum Exploration and Development, CNPC, Beijing 100083, China*; Email: lxz69@petrochina.com.cn

Yong Hu − *School of Engineering Sciences, University of Chinese Academy of Sciences, Beijing 100049, China; Institute of Porous Flow and Fluid Mechanics, Chinese Academy of Sciences, Langfang 065007, China; Research Institute of Petroleum Exploration and Development, CNPC, Beijing 100083, China*; Email: huy69@petrochina.com.cn

Authors

Mengfei Zhou − *School of Engineering Sciences, University of Chinese Academy of Sciences, Beijing 100049, China; Institute of Porous Flow and Fluid Mechanics, Chinese Academy of Sciences, Langfang 065007, China; Research Institute of Petroleum Exploration and Development, CNPC, Beijing 100083, China*; orcid.org/0000-0003-3728-7175

Chang He − *Research Institute of Petroleum Exploration and Development, CNPC, Beijing 100083, China*

Qimin Guo − *Research Institute of Petroleum Exploration and Development, CNPC, Beijing 100083, China*

Yize Huang − *School of Engineering Sciences, University of Chinese Academy of Sciences, Beijing 100049, China; Institute of Porous Flow and Fluid Mechanics, Chinese Academy of Sciences, Langfang 065007, China; Research Institute of Petroleum Exploration and Development, CNPC, Beijing 100083, China*

Xiangyang Pei − *Research Institute of Petroleum Exploration and Development, CNPC, Beijing 100083, China*

Nijun Qi − *School of Engineering Sciences, University of Chinese Academy of Sciences, Beijing 100049, China; Institute of Porous Flow and Fluid Mechanics, Chinese Academy of Sciences, Langfang 065007, China; Research Institute of Petroleum Exploration and Development, CNPC, Beijing 100083, China*

Complete contact information is available at: https://pubs.acs.org/10.1021/acsomega.4c01323

Notes

The authors declare no competing financial interest.

ACKNOWLEDGMENTS

This research was funded by grants 2021DJ1505 and 202DJ1705 from PetroChina.

NOMENCLATURE

Swi initial water saturation, %

r_e well-spacing radius, m

https://doi.org/10.1021/acsomega.4c01323
ACS Omega 2024, 9, 23649−23661

r distance from wellbore, m
p_e initial reservoir pressure, MPa
p reservoir pressure at r, MPa
r_D nondimension distance from the wellbore, dimensionless
p_D nondimension reservoir pressure at r_D, dimensionless
R recovery, %
K permeability, mD
t gas production time

■ ACRONYMS

m meter
min minute

■ REFERENCES

(1) Howarth, R. W. A Bridge to Nowhere: Methane Emissions and the Greenhouse Gas Footprint of Natural Gas. *Energy Sci. Eng.* **2014**, *2* (2), 47−60.
(2) McGlade, C.; Ekins, P. The Geographical Distribution of Fossil Fuels Unused When Limiting Global Warming to 2 °C. *Nature* **2015**, *517* (7533), 187−190.
(3) Davis, S. J.; Socolow, R. H. Commitment Accounting of CO2 Emissions. *Environ. Res. Lett.* **2014**, *9* (8), 084018.
(4) Bellani, J.; Verma, H. K.; Khatri, D.; Makwana, D.; Shah, M. Shale Gas: A Step toward Sustainable Energy Future. *J. Pet. Explor. Prod. Technol.* **2021**, *11* (5), 2127−2141.
(5) Li, X.; Guo, Z.; Hu, Y.; Luo, R.; Su, Y.; Sun, H.; Liu, X.; Wan, Y.; Zhang, Y.; Li, L. Efficient Development Strategies for Large Ultra-Deep Structural Gas Fields in China. *Pet. Explor. Dev.* **2018**, *45* (1), 118−126.
(6) Wei, Y.; Jia, A.; Xu, Y.; Fang, J. Progress on the Different Methods of Reserves Calculation in the Whole Life Cycle of Gas Reservoir Development. *Journal Of Natural Gas Geoscience.* **2021**, *6* (1), 55−63.
(7) Zhao, K.; Zhang, L.; Zheng, D.; Sun, C.; Dang, Q. A Reserve Calculation Method for Fracture-Cavity Carbonate Reservoirs in Tarim Basin, NW China. *Pet. Explor. Dev.* **2015**, *42* (2), 277−282.
(8) Curtis, J. B.; Montgomery, S. L. Recoverable Natural Gas Resource of the United States: Summary of Recent Estimates. *AAPG Bull.* **2002**, *86* (10), 1671−1678.
(9) Zou, C.; Yang, Z.; He, D.; Wei, Y.; Li, J.; Jia, A.; Chen, J.; Zhao, Q.; Li, Y.; Li, J.; et al.et al. Theory, Technology and Prospects of Conventional and Unconventional Natural Gas. *Pet. Explor. Dev.* **2018**, *45* (4), 604−618.
(10) Lee, J.; Sidle, R. Gas-Reserves Estimation in Resource Plays. *SPE Econ. Manage.* **2010**, *2* (2), 86−91.
(11) Walsh, M.; Lake, L. W. *A Generalized Approach to Primary Hydrocarbon Recovery*; Elsevier: Netherlands, 2003.
(12) Lake, L. W.; Johns, R.; Rossen, B.; Pope, G. A. Fundamentals of Enhanced Oil Recovery. In *Displacement Efficiency*; Society of Petroleum Engineers: Richardson, TX, 2014.
(13) Fetkovich, M. J.; Reese, D. E.; Whitson, C. H. Application of a General Material Balance for High-Pressure Gas Reservoirs. *Spe J.* **1998**, *3* (1), 3−13.
(14) King, G. R. Material-Balance Techniques for Coal-Seam and Devonian Shale Gas Reservoirs With Limited Water Influx. *SPE Reservoir Eng.* **1993**, *8* (1), 67−72.
(15) Payne, D. A. Material-Balance Calculations in Tight-Gas Reservoirs: The Pitfalls of p/z Plots and a More Accurate Technique. *SPE Reservoir Eng.* **1996**, *11* (4), 260−267.
(16) Sills, S. R. Improved Material-Balance Regression Analysis for Waterdrive Oil and Gas Reservoirs. *SPE Reservoir Eng.* **1996**, *11* (2), 127−134.
(17) Sun, H.; Wang, H.; Zhu, S.; Nie, H.; Liu, Y.; Li, Y.; Li, S.; Cao, W.; Chang, B. Reserve Evaluation of High Pressure and Ultra-High Pressure Reservoirs with Power Function Material Balance Method. *Nat. Gas Ind. B.* **2019**, *6* (5), 509−516.
(18) Chen, Y.; Qi, Y.; Libing, F.; Yunsheng, W. Methods for Estimating Well-Controlled Movable in-Place and Recoverable Reserves of Shale Gas. *Pet. Geol. Recovery Effic.* **2018**, *25* (4), 73−78.
(19) Liang, H.-B.; Zhang, L.-H.; Zhao, Y.-L.; Zhang, B.-N.; Chang, C.; Chen, M.; Bai, M.-X. Empirical Methods of Decline-Curve Analysis for Shale Gas Reservoirs: Review, Evaluation, and Application. *J. Nat. Gas Sci. Eng.* **2020**, *83*, 103531.
(20) Miao, Y.; Li, X.; Lee, J.; Zhou, Y.; Wu, K.; Sun, Z.; Liu, S. A New Rate-Decline Analysis of Shale Gas Reservoirs: Coupling the Self-Diffusion and Surface Diffusion Characteristics. *J. Pet. Sci. Eng.* **2018**, *163*, 166−176.
(21) Yehia, T.; Abdelhafiz, M. M.; Hegazy, G. M.; Elnekhaily, S. A.; Mahmoud, O. A Comprehensive Review of Deterministic Decline Curve Analysis for Oil and Gas Reservoirs. *Geoenergy Sci. Eng.* **2023**, *226*, 211775.
(22) Fetkovich, M. J.; Vienot, M. E.; Bradley, M. D.; Kiesow, U. G. Decline-Curve Analysis Using Type Curves—Case Histories. *SPE Form. Eval.* **1987**, *2* (4), 637−656.
(23) Chen, Y. Derivation and Application of Weng's Prediction Model. *Nat. Gas Ind.* **1996**, *16* (2), 22−26.
(24) Chen, Y.; Hu, J. Weibull Model for Predicting Output and Reserve in an Oil and Gas Field. *Xinjiang Pet. Geol.* **1995**, *16* (3), 250.
(25) Weibull, W. *Fatigue Testing and Analysis of Results*; Elsevier, 2013.
(26) Chen, Y. *Practical Methods of Petroleum Reservoir Engineering*; Petroleum Industry Press: Beijing, 1999.
(27) Nashawi, I. S.; Malallah, A.; Al-Bisharah, M. Forecasting World Crude Oil Production Using Multicyclic Hubbert Model. *Energy Fuels* **2010**, *24* (3), 1788−1800.
(28) Wang, J.; Jiang, H.; Zhou, Q.; Wu, J.; Qin, S. China's Natural Gas Production and Consumption Analysis Based on the Multicycle Hubbert Model and Rolling Grey Model. *Renewable Sustainable Energy Rev.* **2016**, *53*, 1149−1167.
(29) Hao, M.; Chen, Y.; Zhuang, Y.; Wei, C.; Liu, X. Establishment and Application of the Multi-Peak Forecasting Model. In *IPTC 2013: international Petroleum Technology Conference*; European Association of Geoscientists & Engineers, 2013; cp350.
(30) Hu, J.; Chen, Y.; Zhang, S. A New Model to Predict Production Rate of Oil and Gas Fields. *Acta Petrolei Sinica* **1995**, *16* (1), 79.
(31) Hubbert, M. K. *Energy Resources: A Report to the Committee on Natural Resources of the National Academy of Sciences−National Research Council*; National Academy of Sciences-National Research Council, Washington, DC (USA), 1962. https://www.osti.gov/biblio/5101070 (accessed 2023−10−03).
(32) Li, X.; Liu, X.; Su, Y.; Wu, G.; Liu, H.; Lu, L.; Wan, Y.; Guo, Z.; Shi, S. Correlation between Per-Well Average Dynamic Reserves and Initial Absolute Open Flow Potential (AOFP) for Large Gas Fields in China and Its Application. *Pet. Explor. Dev.* **2018**, *45* (6), 1088−1093.
(33) Hu, Y.; Guo, C.; Xu, X.; Chunyan, J.; Yongqiang, Y. Pore Throat Structure and Flow Characteristics of Sandstone Reservoirs. *Pet. Geol. Exp.* **2015**, *37* (3), 390−393.
(34) Hu, Y.; Li, X.; Lu, X.; Lu, J.; Xu, X.; Jiao, C.; Guo, C. Varying Law of Water Saturation in the Depletion-Drive Development of Sandstone Gas Reservoirs. *Pet. Explor. Dev.* **2014**, *41* (6), 790−793.
(35) Wang, L.; Zhang, Y.; Luo, R.; Zou, R.; Deng, H.; Zou, R.; Huang, L.; Liu, Y. Lower Limits of Petrophysical Parameters for Effective Reservoirs in Ultradeep Carbonate Gas Reservoirs: A Case Study from the Deng IV Member, Gaoshiti-Moxi Area, Sichuan Basin, SW China. *J. Hydrol.* **2023**, *621*, 129657.
(36) Zhou, M.; Xu, X.; Zhang, Y.; Jiao, C.; Tang, Y.; Bi, Z. Experimental Study on Production Performance and Reserve utilization Law in Carbonate Gas Reservoirs. *J. Pet. Explor. Prod. Technol.* **2022**, *12* (4), 1183−1192.
(37) Sun, Z.; Li, X.; Liu, W.; Zhang, T.; He, M.; Nasrabadi, H. Molecular Dynamics of Methane Flow Behavior through Realistic Organic Nanopores under Geologic Shale Condition: Pore Size and Kerogen Types. *Chem. Eng. J.* **2020**, *398*, 124341.
(38) Sun, Z.; Huang, B.; Wang, S.; Wu, K.; Li, H.; Wu, Y. Hydrogen Adsorption in Nanopores: Molecule-Wall Interaction Mechanism. *Int. J. Hydrogen Energy* **2023**, *48* (86), 33496−33508.
(39) Xu, K.; Liang, T.; Zhu, P.; Qi, P.; Lu, J.; Huh, C.; Balhoff, M. A 2.5-D Glass Micromodel for Investigation of Multi-Phase Flow in Porous Media. *Lab Chip.* **2017**, *17* (4), 640−646.

https://doi.org/10.1021/acsomega.4c01323
ACS Omega 2024, 9, 23649−23661

(40) Wang, L.; Yang, S.; Peng, X.; Deng, H.; Meng, Z.; Qian, K.; Wang, Z.; Lei, H. An Improved Visual Investigation on Gas−Water Flow Characteristics and Trapped Gas Formation Mechanism of Fracture−Cavity Carbonate Gas Reservoir. *J. Nat. Gas Sci. Eng.* **2018**, *49*, 213−226.
(41) Xu, X.; Wan, Y.; Li, X.; Hu, Y.; Tian, S.; Mei, Q.; Jiao, C.; Guo, C. Microscopic Imbibition Characterization of Sandstone Reservoirs and Theoretical Model Optimization. *Sci. Rep.* **2021**, *11* (1), 8509.

https://doi.org/10.1021/acsomega.4c01323
ACS Omega 2024, 9, 23649−23661